Application of theory to observed cases of orographically forced convective rainfall

Mario Marcello Miglietta[1]

ISAC-CNR, Lecce, Italy

ISE-CNR, Verbania Pallanza, Italy

Richard Rotunno

NCAR*, Boulder, USA

*The National Center for Atmospheric Research is sponsored by the National Science Foundation.

[1]*Corresponding author address:* Mario Marcello Miglietta, CNR-ISAC, strada provinciale Lecce-Monteroni, 73100 Lecce, Italy.
E-mail: m.miglietta@isac.cnr.it

Abstract

In two recent papers, the authors reported on numerical simulations of conditionally unstable flows past an idealized mesoscale mountain ridge. These idealized simulations, which were performed with a three-dimensional, explicitly cloud-resolving model, allowed the investigation of simulated-precipitation characteristics as a function of the prescribed environment. The numerical solutions were carried out for a uniform wind flowing past a bell-shaped ridge and using an idealized unstable sounding with prescribed values of the relevant parameters.

In the present work the application of these theoretical results to observed cases of orographically forced convective rainfall including the Big Thompson Flood (1976, Colorado), the Oahu Flood (1974, Hawaii), and the Gard Flood (2002, France) is reported. Events occurring in different parts of the world are considered in order to demonstrate the generality of the results. Specifically numerical simulations have been carried out using observed and idealized soundings relevant to these cases but with idealized topography. It is found that using the observed soundings, but with idealized constant wind profiles, the simulated rain rates fit reasonably well within our previous theoretically derived parameter space for intense orographic convective rainfall. However, in order to reproduce larger rainfall rates, in closer agreement with observations, in the first two cases it was necessary to initialize the sounding with a wind profile characterized by low-level flow towards the mountain with weak flow aloft (as observed). For the Gard case, the situation was more complex and it is found unlikely that the situation can be reduced to a simple two-dimensional problem.

1. Introduction

Orographic precipitation results from a complex combination of different scales of motion: moist, large-scale flow, mesoscale orographically induced lifting and small-scale processes such as convection, turbulence, and microphysics (Rotunno and Houze, 2007). While the orographic-precipitation problem in stable and neutral atmospheric conditions is fairly well understood, the problem in the unstable case is still far from being solved and presents significant challenges to the successful numerical prediction of this kind of event.

The occurrence of heavy-rain convective events over complex orography is well documented in different parts of the world (see Richard et al., 2007 for a review). However, the timing, evolution and location of these events can differ greatly from case to case; e.g., the heaviest concentration of rainfall may affect the foothills (Caracena et al., 1979), the region just upwind (Delrieu et al., 2005), or even the downwind side (Schroeder, 1977) of a mountain ridge; in addition, the flow can be deflected by mountain chains or channeled by gaps (Buzzi and Foschini, 2000).

Large rainfall amounts are generally associated with the persistence of convective systems in a limited region for several hours. In such systems, convective cells often have trajectories that carry them over the same location many times (Chappell, 1986, p. 289). For this to occur, outflows from downdrafts either do not move away from the heavy rain, or are not present with the depth nor density difference to initiate cells in locations away from the affected region (Davis, 2001).

Orographic convective triggering and maintenance of such systems has been proposed to occur through different mechanisms, e.g., orographic uplift (Yu et al., 2007), uplift over orographically blocked flow (Neiman et al., 2002; Yu and Hsieh, 2009), formation of areas of convergence (Rotunno and Ferretti, 2001), local convergence at low-level-flow separation lines (Wang et al., 2000), thermal forcing (Romero et al., 2000) and/or the remote effects of mountain waves (Grossman and Durran, 1984). In some cases, the orography serves as a fixed lifting mechanism to force moist flow to its lifting condensation level and "anchors" the system. In addition, the complex nature of the terrain may result in localized areas of persistent convergence that repeatedly triggers convection over the same locations (Kodama and Barnes, 1997).

On the one hand, similarities have been detected in the synoptic environments conducive to some disruptive upslope convective events, such as a short-wave aloft combined with a post-frontal ribbon of high equivalent potential temperature air, and weak middle- and upper-tropospheric currents (Pontrelli et al., 1999). On the other hand, the importance of specifically mesoscale ingredients, such as the moist and conditionally unstable low-level jets, has been examined in particular cases of complex terrain to assess their ability to focus deep convection over the same area for several hours (e.g. the Gard Flood over southern France, see Ducrocq et al., 2008).

Identifying the conditions favorable for a statistically stationary convective system over orography can be particularly difficult, as one can envision scenarios in which deep convective cells do not concentrate their precipitation in the same location. After their formation, cells may move according to the wind aloft and thus produce rain in another location, or, rather, a density current may develop and trigger cells far from the

mountain. In such cases, convectively induced cold pools and outflows can be very important for the propagation of convective systems and/or to focus, together with the orography, convective-cell development in a confined area (Senesi et al., 1996, Romero et al., 2000). A better understanding of the problem first requires the identification of the most important environmental variables. In an attempt to find those parameters in a simplified theoretical context, the authors (Miglietta and Rotunno, 2009, hereafter MR09; Miglietta and Rotunno, 2010, MR10) have recently reported on a series of idealized three-dimensional explicitly cloud-resolving simulations of conditionally unstable flow past a two-dimensional ridge. This study represents our attempt to apply those results to observed cases of intense convective orographic rainfall.

As the analyzed events are generally very complex, due to the three-dimensionality of the flow and of the topography, the time-evolution of the synoptic situation, …, we cannot expect to represent the observed rainfall with the extremely simplified setup we used. Rather, we have tried to apply the results of our previous studies to three soundings, representive of the upstream conditions occurred in heavy rain events, that are somehow different from the Weisman-Klemp (1982) profiles used in those papers, in order to see how well these cases are consistent with our theory. Also, we have explored: how much of the recorded precipitation can be simulated within this simplified context; the sensitivity of the rainfall peak to some of non-dimensional parameters considered in our theory; the importance of an additional parameter, the wind shear, that has not been considered up to now.

In Section 2 we review the theoretical background for the current study. Section 3 recounts our attempts to simulate several well-documented cases within our idealized

context. Section 4 summarizes our conclusions and outlines our view of the next steps to be taken.

2. Theoretical background

As noted above, MR09 and MR10 have recently reported on a series of three-dimensional numerical simulations of conditionally unstable flows impinging on a two-dimensional mesoscale mountain ridge. The simulations were performed with a three-dimensional explicitly cloud-resolving model [Cloud Model 1 (CM1), Bryan and Fritsch (2002)] in order to investigate the statistically stationary (along-ridge averaged) features of the solution precipitation characteristics.

MR09 considered an archetypal sounding for convective instability, the Weisman-Klemp (1982; WK) sounding, with a uniform wind U flowing past a bell-shaped ridge of height h_m and half-width a and specified the Convective Available Potential Energy (CAPE), Downdraft CAPE (DCAPE)[2], Level of Free Convection (LFC), tropopause height h_t, and static stability N^2. MR09 carried out these numerical simulations by varying the different parameters associated with the sounding and with the orography and then measured the convective response in terms of along-ridge averaged rainfall location and intensity.

Dimensional analysis of the results revealed that the maximum non-dimensional rainfall rate $R_m/\rho_{vs}U$, where ρ_{vs} is the saturation vapor density at the ground, mainly depends on three non-dimensional numbers. One is the ratio of mountain height to the level of free convection h_m/LFC, the second is the slope parameter h_m/a, and the third is

[2]DCAPE is a measure of the cold-pool buoyancy produced by rainy downdrafts (see Gilmore and Wicker, 1998)

the ratio of an advective timescale $\tau_a = a/U$ to a convective timescale $\tau_c = h_t/(\text{CAPE})^{1/2}$ (the time that convective elements take to grow and produce rain at the ground; h_t is the height of the tropopause).

With the benefit of tens of simulations, MR09 developed the following conceptual model for large convective orographic rainfall: 1) h_m/LFC should be greater than a threshold value (in order to trigger convection); 2) τ_a/τ_c should not be too large (~ 1-10) (in order to generate a cold pool that will not propagate far away from the ridge) and 3) for given τ_a/τ_c and h_m/LFC~>*0.3,* there is an optimal range of h_m/a (MR09's Fig. 15 and MR10's Figs. 2 and 3).

Subsequently, the work was extended (MR10) to take into account further parameter variations, which were not considered in MR09. Specifically, MR10 extended the MR09 analysis to cover larger regions of the thermodynamic parameter space, in particular covering a wider range of CAPE. MR10 found the precipitation produced in low-CAPE, moderate-wind experiments does not fit the functional dependence for rain rate amount and location proposed in MR09; further analysis suggested that two additional non-dimensional parameters, $\text{DCAPE}^{1/2}/U$ (which represents a measure of the propagation of the downdraft-produced cold pool with respect to environmental-flow advection) and N LFC/U (which estimates the deceleration of the environmental wind induced by the cold pool), should be taken into account.

In order to test the applicability of the above-described work, we have performed a series of three-dimensional high-resolution numerical simulations relevant to observed cases of flooding-rain events using the same simplified context as in our previous studies. The numerical setup is the same as MR09 and MR10, so we will refer to those papers for

further details and limit our description here to the essential information. The domain is 320 km long and 20 km wide with a horizontal grid spacing of 250 m, the vertical extent of the domain is 20 km, with 59 levels having a vertical grid spacing varying from 250 m close to the ground to 500 m in the upper levels. The orography is prescribed by a bell shaped mountain, with small-amplitude irregularities added in order to break the *y*-symmetry of the initial condition and obtain a fully three-dimensional solution. The observed soundings, after some smoothing and simplifications as discussed in Sect. 3, are used to initialize CM1. Thus we will compare the simulations of these observed cases of orographically forced convective rainfall with the theory developed in MR09, MR10.

Finally, as low-level flow towards the orography with weak winds aloft is often present in cases of orographically forced heavy convective rain, we will also perform additional experiments including such wind profiles and consider its effect on the simulated precipitation features. However, for these latter experiments we have not yet developed a theoretical background, since in MR09 and MR10 we had so many parameters to consider that we postponed the analysis of the effect of variable wind $U(z)$ to a future study. Thus, orographic-flow experiments with the prototypal Weisman-Klemp sounding, but with typical wind profiles $U=U(z)$, will be discussed in a following article.

3. Case studies

In the present Section, different case studies with strong orographic convection are analyzed and discussed in the framework of the theory developed in MR09 and MR10. Events that occurred in different parts of the world are considered in order to demonstrate the generality of the results.

The present endeavor presented several challenges. Generally, the meteorological situation is non-stationary and spatially varying and the topography is three-dimensional; thus the idealization of using a single sounding upstream of a two-dimensional mountain can be an over-simplification of the problem. However even if one stipulates the applicability of a single sounding, the results can still be quite sensitive to what may appear to be minor variations in the sounding. Herein we present an account of our attempts to use real soundings with simplified orography to see if one can describe at least the gross features of observed orographic convective heavy-rain events.

In the observed cases only the maximum instantaneous rain rate of a cell with limited duration is reported. In the simulations, a statistically steady state is established which, by definition, is of infinite duration. Thus it is not possible to establish a one-to-one correspondence between observed and simulated rainfall peak R_m. However we can compare different simulations to each other and ask which produces the largest R_m for sounding variations within the observed range of variability and thus assess what conditions might have led to the largest rain rates and presumably intense rainfall in the observed cases. Flooding, however, is a result of repeating rain cells over a specific location; in the case of orographic precipitation, the distance from the summit of the maximum statistically steady rain rate, X_m, is the appropriate datum for comparison with the observed region of flooding rains.

a. Big Thompson

First we consider the Big Thompson Canyon (BIGT) flood, which involved orographically forced convection over the Rocky Mountains as discussed in Caracena et al. (1979). The BIGT case was characterized by a strong low-level easterly flow, oriented

nearly normal to the orography, that advected a very moist, conditionally unstable air mass towards the eastern side of Front Range of the Rocky Mountains, about 40 km north of Boulder, Colorado on 31 July/1 August 1976 (Fig.1). According to Caracena et al. (1979) orographic uplift provided the necessary destabilization to trigger convection, and a very light upper-level southerly wind allowed the storm complex to remain nearly stationary. Heavy precipitation focused on a narrow corridor in the foothills, producing devastating flash floods, while no intense precipitation occurred at higher elevations. At least 139 people were killed and property damage of about $ 35.5 million occurred. A detailed analysis of the synoptic conditions of the pre-storm stage can be found in Maddox et al. (1978).

1) EXPERIMENTS WITH U = CONST

In our preliminary attempts using the smoothed profile reported in Yoshizaki and Ogura (1988)'s Fig. 2a and the constant wind U = 13 m s^{-1}, we found that the rainfall rate (Exp. BIGT1 in Tab. I) was much smaller than that indicated by the observations [Caracena et al. (1979) calculated adjusted rainfall rates $\sim$ 150 mm h^{-1} in the flooding area during the most intense part of the storm]. In a further attempt, we initialized the model with the interpolated sounding (representative of upstream conditions), shown in Caracena et al. (1979)'s Fig. 5b and the constant wind U = 10 m s^{-1} (Exp. BIGT2 in Tab. I). Also in this case the rainfall rate was very small.

However, that sounding contains some thermal inversions, which could prevent the triggering of convection, and very dry midlevels, which would produce overly strong cold pools; thus we decided to initialize the model with our own smoothed profiles shown in Fig. 2. We used U = 10 m s^{-1}, the average wind throughout the vertical column, and a

bell-shaped mountain with h_m = 1800 m and a = 30 km (Exp. BIGT3 in Tab. I). We tested also slight increases in the humidity content between 800 and 700 hPa (Exp. BIGT4 in Tab. I and dashed lines in Fig. 2), or a different mountain shape (the same upstream width but with a downstream width twice as large, Exp. BIGT5, thus closer to the real mountain shape), but in all cases the rainfall peak was much smaller than observed, of about 10 mm h^{-1}.

Based on the findings in MR09 and MR10, we looked for slight variations in the parameters U, h_m, and a (but still reasonably close to those of the BIGT case) that would produce stronger precipitation. As shown in Tab. I, the two simulations BIGT6 (U = 10 m s^{-1}) and BIGT7 (U = 7 m s^{-1}) belong to a region of large h_m/a and h_m/LFC for small/intermediate τ_a/τ_c (cf. MR10's Fig. 3). With respect to Exp. BIGT3, these two experiments had slightly increased the rainfall, due to the presence of deeper convective cells, and the peak is shifted downstream. In particular, in Exp. BIGT7, a smaller wind speed produced a larger non-dimensional rainfall, although the changes in absolute precipitation were relatively minor.

To evaluate how much the choice of the value of the constant wind affected the rainfall rate, we performed three additional experiments with exactly the same setup but with the different wind speeds U = 5 m s^{-1}, 10 m s^{-1} and 17 m s^{-1} (Exp. BIGT9, BIGT10, BIGT11). In Exp. BIGT9, a cold pool propagated far upstream and no stationary rainfall was simulated above the mountain. Both the other two cases show results similar to the previous experiments with uniform wind profiles; Figs. 3a-b illustrate the solution for the case BIGT10. (The main difference between BIGT10 and BIGT11 is the distribution of the precipitation, which is shifted downstream in the latter case with stronger winds.)

2) EXPERIMENTS WITH $U = U(Z)$

Considering that the observations show an intense low-level flow towards the mountains with weaker across-mountain flow aloft, we decided to introduce a similar wind profile in the initial condition. Using the same sounding as in Exp. BIGT10, we initialized the model with a wind profile having $U = 17$ m s^{-1} in the lowest 4 model levels (1500-2400 m) and $U = 0$ m s^{-1} above 4000 m (from level 11 above), with a linear interpolation defining $U(z)$ in between. The presence of the low-level flow dramatically increases the rainfall rate and the rainfall maximum is now located farther upstream (Exp. BIGT8 in Tab. I). Figures 3c-d show that this outcome is due to the presence of deep convective cells on the upstream side of the mountain, which are generated upstream as a consequence of lifting induced by a deep cold pool [the presence of a cold air pool caused by the evaporative cooling had been noted in the simulations in Yoshizaki and Ogura (1988)]. The presence of a low-level flow and calm aloft thus appear to be fundamental ingredients for the occurrence of larger rainfall rates in the simulations of this case (as concluded/hypothesized in observational studies).

The comparison of the constant-wind Exp. BIGT10 with the low-level-flow-only Exp. BIGT8 in Fig. 3, shows that the two solutions have a completely different behavior. In Exp. BIGT10 (Fig. 3, top), the wind field indicates the presence of a mountain wave that warms the upper levels (by about 3 K, not shown) downstream and above the mountain, while Exp. BIGT8 (Fig. 3, bottom) is characterized by a cold pool remaining on the mountain with no mountain wave in evidence. In the latter case, the uplift induced

by the cold pool, together with the absence of upper-level advection, produce deep convective cells and shift the rainfall peak farther upstream.

To test the sensitivity of the solution to the value of the low-level flow, Exp. BIGT12 was done with the same numerical setup as in Exp. BIGT8, but with $U = 10$ m s^{-1} instead of $U = 17$ m s^{-1} in the lower layer. In this case, a cold pool propagated upstream and thus no stationary rainfall occurred near the mountain.

Two main conclusions can be drawn from these simulations. First, our BIGT experiments with constant environmental wind seem to fit pretty well with the theory developed in MR09 and MR10 (see Tab. I). In fact, the points corresponding to Exp. BIGT3, BIGT4, BIGT5 and BIGT10 fall in the region on the right side in MR09's Figs. 15b and 16b, and behave accordingly, as they show intermediate rainfall rates and slightly upstream rainfall peaks; Exp. BIGT6, BIGT7 and BIGT11 agree well with MR10's Fig.3, as they belong to a region of the parameter space characterized by moderate/large (BIGT6 and BIGT7) or moderate/small (BIGT11) downstream rainfall peaks; BIGT9 corresponds correctly to a region of non-stationary rainfall (MR09's Fig. 15c). However, the estimated rainfall rates for the BIGT case are too small compared with observed values[3].

It appears that the inclusion of a low-level flow with no flow aloft produces deeper convective cells and a larger rainfall rate, and it puts the precipitation maximum on the upstream side of the mountain in this case. However, Exp. BIGT9 and BIGT12 show that the low-level flow should be a proper combination of depth and intensity in order to produce an increase in the precipitation rate; too weak a wind speed or too

[3]However, here the maximum amount represents the longitudinal average across the channel and not the rainfall associated with a single system as in Caracena et al. (1979).

shallow a layer of low-level flow does not stop the cold pool from propagating away from the mountain.

b. Oahu case

In this section we describe our simulations of the Oahu (Hawaii) flood of 1974 (Schroeder, 1977). This case was chosen in order to explore rather different environmental conditions, in an area vulnerable to heavy rain events (Kodama and Barnes, 1977; Lyman et al., 2005, among the others); the topography, characterized by very steep slopes (Fig. 4), has different characteristic lengths from that of the Rockies in the area of the Big Thompson flood, and in contrast to the BIGT case, while the thunderstorms initiated at the ridge, the flooding occurred downwind of the ridge crest.

The flash floods caused by heavy thunderstorms on the morning of 19 April 1974 resulted in five deaths and $ 3.9 million property damage in the Hawaiian islands. A peak rain rate of 114 mm in 1 h and a rainfall amount of 267 mm in 4 h was recorded on the northern side of the island (Schroeder, 1977).

As in the BIGT case, the OAHU case is characterized by persistent, moderate easterly low-level flow towards the orography, however we initially considered a sounding with a constant wind $U = 10$ m s^{-1}. This value is comparable to the mean across-mountain wind component, calculated from the vertical profile below 500 hPa at 0200 local time (= UTC - 10), 19 April 1974, in Schroeder (1977)'s Fig. 5.

We started our analysis by initializing the model with the sounding from Lihue (21.98°N, 159.35°W; on the eastern side of Kauai island, west-north-west of Oahu) at 12 UTC, 19 April 1974, downloaded from the University of Wyoming website (http://weather.uwyo.edu/upperair/sounding.html). The sounding appeared to be

absolutely unstable; consequently, our numerical simulation exhibited a large amount of convection everywhere in the domain. In a personal communication, T. Schroeder was of the opinion that the original sounding was not accurate[4]. Thus, we decided to initialize our model with the sounding in Schroeder (1977)'s Fig. 6, modified by a slight smoothing (temperature and dewpoint temperature represented by the dashed lines in Fig. 5). A bell-shaped mountain with h_m = 1000 m and a = 10 km was used. Our numerical simulations indicated weak precipitation compared to the observations [cf. Exp. OAHU1 in Tab. II with the observed peak of approximately 50-100 mm h^{-1} during the period of the most intense rainfall, as shown in Schroeder (1977, his Fig. 8)], while the maximum occurred slightly upstream of the mountain crest instead of the observed downstream location. To see if small changes in the sounding would produce larger rainfall rates, we removed the thermal inversion from 600 hPa to 450 hPa (solid-line temperature profile with dashed-line dewpoint temperature profile in Fig. 5), which also had the effect of slightly increasing the value of CAPE (Exp. OAHU2 in Tab. II); again, the simulated convection was weak and the results from Exp. OAHU1 were only marginally changed.

Taking into consideration the uncertainties in the humidity sounding, in the next experiment the dew point was increased with respect to Exp. OAHU1 in the layer from 950 hPa to 600 hPa (Exp. OAHU3 in Tab. II; dashed-line temperature profile with solid-line dew point profile in Fig. 5). As a result, a much larger rainfall rate (15 mm h^{-1}) was generated in the simulation, but the location of the maximum was still confined mainly upstream of the crest. Finally, when the modifications to both dew point and temperature were included in the sounding (solid lines in Fig. 5; Exp. OAHU4 in Tab. II), the

[4]"This is pure speculation but it may be possible that the soundings were later adjusted ... I recall there was some 'flap' about humidity sensors on NWS sondes back in the 70's..." (see also Wade, 1994).

precipitation rate did not change with respect to Exp. OAHU3 (thus the change in dew point determines the major modification with respect to Exp. OAHU1), while the rainfall maximum was mainly confined to the mountain crest.

In order to compare the model results with the theoretical results in MR09 and MR10, we note that the present simulations show a rainfall peak located mainly at the ridge crest or slightly upstream, consistent with MR10's Fig. 2b (h_m/a = 0.10, h_m/LFC = 1.0 - 1.25). Concerning the rainfall rate, the comparison is more complex, however the progressive increase of the non-dimensional rainfall in Exp. OAHU1-4 with increasing τ_a/τ_c is consistent with the rightward shift of the maximum non-dimensional rainfall in going from MR10's Fig.2a (τ_a/τ_c = 3.3) to MR10's Fig.3a (τ_a/τ_c = 6.6).

As for the BIGT simulations, we have found that a key factor in the OAHU case is the presence of low-level flow towards the orography and relatively light cross-barrier flow aloft. Again, when we considered a simulation with low-level flow and no flow aloft, the precipitation rate was much larger (Exp. OAHU5 in Tab. II). The setup of Exp. OAHU5 differs from Exp. OAHU4 only in terms of the wind profile: the wind speed is the same below 2900 m (U = 10 m s^{-1}), while above 4200 m it is equal to 0 (the profile was derived from the observations of the upstream across-mountain wind component); between 2900 m and 4200 m, $U(z)$ is determined by a linear interpolation. As in the BIGT case the simulation with the above-described wind profile $U(z)$ increases the precipitation peak by a factor of more than 2 and it also shifts the simulated peak to the downwind side of the ridge crest, in better agreement with the observations.

Comparing simulations with U = const and with $U = U(z)$ in Fig. 6 one sees that the latter favors the vertical development of convective cells (Figs. 6c-d), while in the

constant-wind case, Figs. 6a-b show that their vertical extent is more confined. Compared to the BIGT case, the cold pool in the $U = U(z)$ case is weaker (limited evaporative cooling was also noted in Schroeder, 1977) and confined downstream of the ridge. Also, the lee-side downward motion associated with the presence of a mountain wave in the OAHU4 case (Figs. 6a-b) suppresses the rainfall there (cf. Smith et al., 2009) and thus shifts the precipitation pattern upstream. As a consequence, in Exp. OAHU5 the rainfall occurs downwind of the ridge crest, while in Exp. OAHU4 the main maximum is confined to a very limited area at the ridge crest (and to a secondary maximum farther downstream associated with the 'hydraulic-jump' feature; see MR09, p. 1874). Finally, in Exp. OAHU5 the simulated precipitation is more uniformly distributed along the mountain with some weak bands upstream of the mountain peak, while in Exp. OAHU4 the rainfall is concentrated in banded features (Fig. 7), similar to those studied in Kirshbaum et al. (2007a, 2007b).

c. Gard

This case has been studied in several papers (Delrieu et al., 2004; Davolio et al., 2006; Nuisser et al., 2008; Ducrocq et al., 2008; Bresson et al., 2009; Davolio et al., 2009 among others). The area affected by the flood was Gard, France, in the Cévennes–Vivarais region. The latter is characterized by a complex orography, the Cévennes mountains, elongated for about 60 km from southwest to northeast, with a maximum peak of about 1700 m (Fig. 8).

The 8-9 September 2002 flash flood resulted in 24 casualties and economic damage of about € 1.2 billion. The event was particularly remarkable for the spatial extent of the rainfall, which was greater than 200 mm in 24 h over 5500 km^2, and its

maximum daily values of 600-700 mm, with a peak of 140 mm h^{-1} (Delrieu et al., 2004). Most of the intense rainfall amount occurred slightly upstream in connection with a quasi-stationary mesoscale convective system.

The region was affected by a persistent moist and warm low-level flow. However, the meteorological features characterizing the event are significantly three-dimensional, as the southerly flow from the Mediterranean Sea, which affects the southern part of the region, interacts with an easterly flow affecting its northern part (Nuisser et al., 2008) in proximity of highly complicated three-dimensional mountain barriers. Also, the situation is non-stationary, as the episode underwent three distinct phases, during which the large-scale circulation changed significantly (among the other factors, a cold front crossed the area from the west).

Thus, the limitations previously discussed were particularly relevant for this case study and it was difficult to identify one single sounding that could be considered representative of the atmospheric conditions upstream of the event. For lack of a better alternative to study this case in the present simplified framework, we initialized the model with the sounding from Nimes (43.86°N, 4.40°E) at 12 UTC, 08 September 2002 (the same as that chosen in Bresson et al., 2009), with a constant wind speed U = 10 m s^{-1} (Fig. 9) and we used a bell-shaped mountain with h_m = 1500 m and a = 30 km (Exp. GARD1 in Tab. III). The result was a very small rainfall rate on the upstream side of the obstacle. In order to compare the simulation with the results shown in Bresson et al. (2009) (their UNIHU simulation), we increased the wind speed to U = 15 m s^{-1} (Exp. GARD2 in Tab. III). Rainfall rate increases and the model results (upstream quasi-stationary cells in Fig. 10a) qualitatively resemble those shown in Bresson et al. (2009)'s

Figs. 3 and 6. Moreover, both Exp. GARD1 and Exp. GARD2 fit well with MR10's Fig. 2, as the corresponding points in the parameter space belong to a region of relatively small non-dimensional rainfall (~ 1) and upstream location of the peak.

Motivated by the present experience with the BIGT and OAHU simulations, we tested the role of a wind profile *U(z)*, by setting $U = 15$ m s^{-1} below 3400 m and $U = 0$ above 5500 m, which reproduces the observed vertical profile of the across-mountain wind component (Exp. GARD3 in Tab. III).

Figure 10 compares the constant-wind case Exp. GARD2 (top) with low-level-flow-only case Exp. GARD3 (bottom): stationary rainfall was simulated upstream of the mountain in both cases, and the rainfall rate was similar in the two experiments (Tab. III). A notable difference with respect to the BIGT and OAHU simulations is that no cold pool is generated[5] (this is a consequence of the small values of DCAPE) and relatively shallow convective cells. The main change due to the wind profile *U(z)* is the removal of the gravity-wave structure in the upper levels above the mountain (the wave structures is in evidence below ~5 km, see Fig. 10c). In contrast with the OAHU case, along-flow rainbands are apparent in both Exp. GARD2 and GARD3 (not shown): thus we infer that the development of deep convection with a cold pool and the elimination of mountain waves are necessary in order to remove the bands and makes the precipitation more uniform in the along-mountain direction (consistent with Kirshbaum et al., 2007a, 2007b).

In order to look for an optimal wind configuration that could significantly enhance the precipitation rate, additional experiments with different wind profiles were

[5]The presence of a cold pool in the simulations in Ducrocq et al. (2008) and Davolio et al. (2009) suggests that our idealization is too simple to reproduce this case study. The sensitivity experiments in Nuisser et al. (2008) provide some indications of the three-dimensional factors that should be taken into account.

performed. For example, we set U = 15 m s^{-1} below 2700 m and U = 0 above 4700 m (Exp. GARD4 in Tab. III) – i.e. slightly reducing the depth of the low level jet with respect to Exp. GARD3-, while in Exp. GARD5 (Tab. III) we initialized the model with the same wind profile used in Exp. OAHU5. However, none of these simulations showed any relevant change in the solution characteristics. Thus, our conclusion is that in this low-CAPE/DCAPE case the presence of the low-level flow with weak winds aloft does not significantly affect the precipitation in our simplified numerical experiments.

4. Conclusions

In the present paper we examined several idealized simulations relative to case studies of orographic convective heavy rainfall, which were performed using a setup basically as that described in Miglietta and Rotunno (2009). Here we used a constant wind profile and profiles of temperature and humidity representative of the observed upstream environmental conditions, somehow different from the Weisman-Klemp sounding used in our previous idealized studies.

We obtained results in line with the dimensional analysis discussed in Miglietta and Rotunno (2009, 2010). However, with respect to the observations, much smaller rainfall rates were simulated due to the over-simplification of the problem. We found that the uniform wind profiles used to initialize the model had to be modified in order to obtain larger rainfall rates. Specifically we found that low-level flow towards the mountain with weak wind aloft can double simulated rain rates.

Our basic point of reference is the case of Big Thompson flood. In this case, we considered a constant-wind profile, and found that the simulated precipitation characteristics agree fairly well with the theory developed in MR09-MR10, but did not fit

well with the observations. We tried to modify different parameters in the thermodynamic sounding within observational uncertainty, but we could not obtain anything significantly different. A major difference came when we considered a sounding with a low-level flow towards the mountain and decreasing to zero aloft. With the latter wind profile, the simulated precipitation is in the correct location, upstream of the mountain ridge, and intense (although much smaller than the observations). When we considered the same wind profile but with a weaker low-level flow, the simulation produced a cold pool propagating away from the mountain and, in that case, no steady-state solution was obtained.

Other cases were then analyzed. The Oahu case showed results basically consistent with the Big Thompson case. On the other hand, for the Gard case, the wind shear was not able to significantly intensify the rainfall. We believe that this lack of influence of wind shear is due to the very small CAPE, thus the convection is shallow and the cell development cannot benefit for the weaker wind aloft; also DCAPE is small, thus the cold pool, which in the other two cases with wind shear was generally deep and remained confined close to the mountain, was very weak.

Although not reported on here, in an attempt to explore more general situations we analyzed other two episodes of orographic convective rainfall. In one case, we considered a sounding representative of heavy-rain conditions over the south-facing (upstream) slopes of island of Hawaii (sounding in Lihue of 19 November 2000, 00 UTC; see Kodama and Barnes, 1977). In another case, we considered a sounding of 31 May 2008 from the Terrain-influenced Monsoon Rainfall Experiment (TiMREX), a field program conducted in the complex orography regions of southern Taiwan in 2008. In

both cases, the low-level jet and calm aloft is effective in more than doubling precipitation.

The larger rainfall in the simulations with shear can be attributed to two different factors: 1) convective cells are deeper and stronger than those in the constant-wind case and 2) cells are not moving with respect to the mountain (this factor is usually mentioned in observational studies), as the cells go up into upper layers characterized by very weak wind, they are no longer advected with respect to the mountain and thus produce a more stationary rainfall pattern.

The effect of the wind profile will be explored more deeply in a following article where we will report on experiments using the Weisman-Klemp sounding but with shear profiles consistent with the present case-study simulations. The primary results are that the orographic-precipitation characteristics of the solutions are the result of a balance between the cold-pool propagation away from the mountain and advection by the environmental wind toward it. In addition, compared to the cases with constant wind, the presence of low-level shear produces deeper and more intense updrafts, stronger cold pools, and locally heavier precipitation as described in Rotunno et al. (1988), Weisman and Rotunno (2004) and Bryan et al. (2006).

References

Bresson, R., D. Ricard, and V. Ducrocq, 2009: Idealized mesoscale numerical study of Mediterranean heavy precipitating convective systems. *Meteor. Atmos. Phys.,* **103,** 45-55.

Bryan, G. H., and J. M. Fritsch, 2002: A benchmark simulation for moist nonhydrostatic models. *Mon. Wea. Rev.,* **130**, 2917-2928.

Bryan, G. H., J. C. Knievel, and M. D. Parker, 2006: A Multimodel Assessment of RKW Theory's Relevance to Squall-Line Characteristics. *Mon. Wea. Rev.,* **134**, 2772-2792.

Buzzi, A., and L. Foschini, 2000: Mesoscale meteorological features sssociated with heavy precipitation in the southern Alpine region. *Meteor. Atmos. Phys.,* **72**, 131-146.

Caracena, F.R., A. Maddox, L. R. Hoxit, and C. F. Chappell, 1979: Meso-analysis of the Big Thompson storm. *Mon. Wea. Rev.,* **107**, 1–17.

Chappell, C. F., 1986: Quasi-stationary convective events. *Mesoscale meteorology and forecasting.* P. S. Ray, Ed., Amer. Meteor. Soc., 289–310.

Davis, R. S., 2001: Flash flood forecast and detection methods. *Severe Convective Storms, Meteor. Monogr.,* No. 50, Amer. Meteor. Soc., 481-525.

Davolio, S., A. Buzzi, and P. Malguzzi, 2006: Orographic influence on deep convection: case study and sensitivity experiments. *Meteor. Zeit.,* **15**, 215-223.

Davolio, S., A. Buzzi, and P. Malguzzi, 2009: Orographic triggering of long-lived convection in three dimensions. *Meteor. Atmos. Phys.,* **103,** 35-44.

Delrieu, G., V. Ducrocq, E. Gaume, J. Nicol, O. Payrastre, E. Yates, P.-E. Kirstetter, H. Andrieu, P.-A. Ayral, C. Bouvier, J.-D. Creutin, M. Livet, S. Anquetin, M. Lang, L. Neppel, C. Obled, J. Parent du Châtelet, G.-M. Saulnier, A. Walpersdorf, and W. Wobrock, 2005: The catastrophic flash-flood event of 8-9 September 2002 in the Gard

region, France: a first case study for the Cévennes-Vivarais Mediterranean Hydrometeorological Observatory. *J. Hydrometeor.,* **6**, 34–52.

Ducrocq, V., O. Nuissier, D. Ricard, C. Lebeaupin, and T. Thouvenin, 2008: A numerical study of three catastrophic precipitating events over western Mediterranean region (southern France). Part II: Mesoscale triggering and stationarity factors. *Quart. J. Roy. Meteor. Soc.,* **34**, 131–145.

Gilmore, M., and L. J. Wicker, 1998: The influence of midtropospheric dryness on supercell morphology and evolution. *Mon. Wea. Rev.,* **126**, 943–958.

Grossman, R. L., and D. R. Durran, 1984: Interaction of low-level flow with the western Ghat mountains and offshore convection in the summer monsoon. *Mon. Wea. Rev.,* **112**, 652–672.

Kirshbaum, D. J., G. H. Bryan, R. Rotunno, and D. R. Durran, 2007a: The triggering of orographic rainbands by small-scale topography. *J. Atmos. Sci.,* **64**, 1530-1549.

Kirshbaum, D. J., R. Rotunno, and G. H. Bryan, 2007b: The spacing of orographic rainbands triggered by small-scale topography. *J. Atmos. Sci.,* **64**, 4222-4245.

Kodama, K., and G. M. Barnes, 1997: Heavy Rain Events over the South-Facing Slopes of Hawaii: Attendant Conditions. *Wea. Forecasting,* **12**, 347–367.

Lyman, R. E., T. A. Schroeder, and G. M. Barnes, 2005: The Heavy Rain Event of 29 October 2000 in Hana, Maui. *Wea. Forecasting,* **20**, 397–414.

Maddox, R. A., L. R. Hoxit, C. F. Chappell, F. Caracena, 1978: Comparison of meteorological aspects of the Big Thompson and Rapid City flash floods. *Mon. Wea. Rev*., **106**, 375-389.

Miglietta, M. M., and R. Rotunno, 2009: Numerical simulations of conditionally unstable flows over a ridge. *J. Atmos. Sci.,* **66**, 1865-1885.

Miglietta, M. M., and R. Rotunno, 2010: Numerical Simulations of Low-CAPE Flows over a Mountain Ridge. *J. Atmos. Sci.,* **67**, 2391-2401.

Neiman, P. J., F. M. Ralph, A. B. White, D. E. Kingsmill, and P. O. G. Persson, 2002: The Statistical Relationship between Upslope Flow and Rainfall in California's Coastal Mountains: Observations during CALJET. *Mon. Wea. Rev.,* **130**, 1468–1492.

Nuissier, O., V. Ducrocq, D. Ricard, C. Lebeaupin, and S. Anquetin, 2008: A numerical study of three catastrophic precipitating events over Southern France. I: Numerical framework and synoptic ingredients. *Quart. J. Roy. Meteor. Soc.,* **134**, 111–130.

Pontrelli, M. D., G. H. Bryan, and J. M. Fritsch, 1999: The Madison County, Virginia, flash flood of 27 June 1995. *Wea. Forecasting,* **14**, 384-404.

Richard, E., A. Buzzi, and G. Zängl, 2007: Quantitative precipitation forecasting in the Alps: The advances achieved by the Mesoscale Alpine Programme. *Quart. J. Roy. Meteor. Soc.,* **133**, 831-846.

Romero, R., C. A. Doswell III, and C. Ramis, 2000: Mesoscale Numerical Study of Two Cases of Long-Lived Quasi-Stationary Convective Systems over Eastern Spain. *Mon. Wea. Rev.,* **128**, 3731-3751.

Rotunno, R., J. B. Klemp, and M. L. Weisman, 1988: A theory for strong, long-lived squall lines. *J. Atmos. Sci.,* **45**, 463–485.

Rotunno, R., and R. Ferretti, 2001: Mechanisms of intense Alpine rainfall. *J. Atmos. Sci.,* **58,** 1732–1749.

Rotunno, R., and R. A. Houze, 2007: Lessons on orographic precipitation from the Mesoscale Alpine Programme. *Quart. J. Roy. Meteor. Soc.,* **133**, 811–830.

Schroeder, T. A., 1977: Meteorological Analysis of an Oahu Flood. *Mon. Wea. Rev.,* **105**, 458-468.

Senesi, S., P. Bougeault, J.-L. Chèze, P. Cosentino, and R.-M. Thepenier, 1996: The Vaison-La-Romaine flash flood: mesoscale analysis and predictability issues. *Wea. Forecasting,* **11**, 417-442.

Smith, R. B., P. Schafer, D. J. Kirshbaum, and E. Regina, 2009: Orographic Precipitation in the Tropics: Experiments in Dominica. *J. Atmos. Sci.,* **66**, 1698-1716.

Yoshizaki, M., and Y. Ogura, 1988: Two- and three-dimensional modelling studies of the Big Thompson storm. *J. Atmos. Sci.,* **45**, 3700-3722.

Yu, C.-K., D. P. Jorgensen, and F. Roux, 2007: Multiple Precipitation Mechanisms over Mountains Observed by Airborne Doppler Radar during MAP IOP5. *Mon. Wea. Rev.* **135**, 955–984.

Yu, C.-K., and Y.-H. Hsieh, 2009: Formation of the Convective Lines off the Mountainous Coast of Southeastern Taiwan: A Case Study of 3 January 2004. *Mon. Wea. Rev.,* **137**, 3072–3091.

Wade, C. G., 1994: An evaluation of problems affecting the measurements of low relative humidity on the United Stated radiosondes. *J. Atmos. Oceanic Technol.,* **11**, 687-700.

Wang, J.-J., R. M. Rauber, H. T. Ochs III, and R. E. Carbone, 2000: The Effects of the Island of Hawaii on Offshore Rainband Evolution. *Mon. Wea. Rev.,* **128,** 1052-1069.

Weisman, M. L., and J. B. Klemp, 1982: The dependence of numerically simulated convective storms on vertical wind shear and buoyancy. *Mon. Wea. Rev.,* **119,** 504-520.

Weisman, M. L., and R. Rotunno, 2004: "A theory for strong long-lived squall lines" revisited. *J. Atmos. Sci.,* **61**, 361–382.

List of Figures

FIG. 7. Rainfall rates simulated near the mountain in experiments OAHU4 (a, top) and OAHU5 (b, bottom). The rainfall is calculated as the hourly average from t = 5 to t = 10 h. The vertical line represents the location of the ridge top.

FIG. 8. As Fig. 1, but for the Gard flash-flood.

FIG. 9. The idealized profiles of temperature and dew point used in our experiments GARD1-5 (solid, thick black lines). The bolded grey line represents the pseudo-adiabatic curve of a parcel lifted from the surface.

FIG. 10. As Fig. 6, but for experiments GARD2 (top) and GARD3 (bottom).

TABLE 1. List of experiments relative to BIGT case. The simulations are identified with the number of the experiment, the value of U, h_m, a , CAPE, DCAPE, LFC, N. The five nondimensional parameters identified in MR09 and MR10 (τ_a/τ_c, h_m/a, $h_m/$LFC, $($DCAPE$)^{1/2}/U$, N LFC$/U$), the values of the rainfall peak R_m and its location X_m are also shown together with the nondimensional parameters $10^2 R_m/\rho_{v,s}U$ and X_m/a.

EXP	U	h_m	a	CAPE	DCAPE	LFC	N	τ_a/τ_c	h_m/a	h_m/LFC	$(DCAPE)^{0.5}/U$	N LFC/U	R_m	X_m	$10^2 R_m/\rho U$	X_m/a
units	m/s	m	km	J/kg	J/kg	m	1/s						mm/h	km		
BIGT1	13	1800	30	1550	920	1000	0,008	9,1	0,06	1,80	2,3	0,6	2	1	0,4	0,0
BIGT2	10	1800	30	2350	1020	2000	0,008	14,5	0,06	0,90	3,2	1,6	1	-8	0,2	-0,3
BIGT3	10	1800	30	2300	1013	1500	0,01	14,4	0,06	1,20	3,2	1,3	8	-6	1,8	-0,2
BIGT4	10	1800	30	2500	1017	1500	0,01	15,0	0,06	1,20	3,2	1,3	8	-6	1,8	-0,2
BIGT5	10	1800	30	2500	1017	1500	0,01	15,0	0,06	1,20	3,2	1,3	9	-13	2,1	-0,4
BIGT6	10	2000	13	2300	1013	1500	0,01	6,2	0,15	1,33	3,2	1,3	10	13	2,3	1,0
BIGT7	7	2000	13	2300	1013	1500	0,01	8,9	0,15	1,33	4,5	1,8	8	4	2,6	0,3
BIGT8		2000	30	2500	1017	1500	0,01		0,07	1,33			19	-19		-0,6
BIGT9	5	2000	30	2500	1017	1500	0,01	30,0	0,07	1,33	6,4	2,6	0		0,0	0,0
BIGT10	10	2000	30	2500	1017	1500	0,01	15,0	0,07	1,33	3,2	1,3	8	-8	1,8	-0,3
BIGT11	17	2000	30	2500	1017	1500	0,01	8,8	0,07	1,33	1,9	0,8	11	10	1,5	0,3
BIGT12		2000	30	2500	1017	1500	0,01		0,07	1,33			0			

TABLE 2. as Tab. 1, but for the OAHU case.

EXP	U	h_m	a	CAPE	DCAPE	LFC	N	T_a/T_c	h_m/a	h_m/LFC	$(DCAPE)^{0.5}/U$	N LFC/U	R_m	X_m	$10^2 R_m/\rho U$	X_m/a
units	m/s	m	km	J/kg	J/kg	m	1/s						mm/h	km		
OAHU1	10	1000	10	650	650	1000	0,01	2,5	0,10	1,00	2,5	0,8	5	-1	1,0	-0,1
OAHU2	10	1000	10	850	650	1000	0,01	2,9	0,10	1,00	2,5	0,8	4	-3	0,8	-0,3
OAHU3	10	1000	10	950	560	800	0,01	3,1	0,10	1,25	2,4	0,6	15	-3	3,0	-0,3
OAHU4	10	1000	10	1150	605	800	0,008	3,4	0,10	1,25	2,5	0,6	16	0	3,2	0,0

TABLE 3. as Tab. 1, but for the GARD case.

EXP	U	h_m	a	CAPE	DCAPE	LFC	N	T_a/T_c	h_m/a	h_m/LFC	$(DCAPE)^{0.5}/U$	N LFC/U	R_m	X_m	$10^2 R_m/\rho U$	X_m/a
units	m/s	m	km	J/kg	J/kg	m	1/s						mm/h	km		
GARD1	10	1500	30	180	200	1500	0,01	4,0	0,05	1,00	1,4	1,8	5	-19	1,0	-0,6
GARD2	15	1500	30	180	200	1500	0,01	2,7	0,05	1,00	0,9	1,2	8	-10	1,1	-0,3
GARD3		1500	30	180	200	1500	0,01		0,05	1,00			11	-9		-0,3
GARD4		1500	30	180	200	1500	0,01		0,05	1,00			11	-16		-0,5

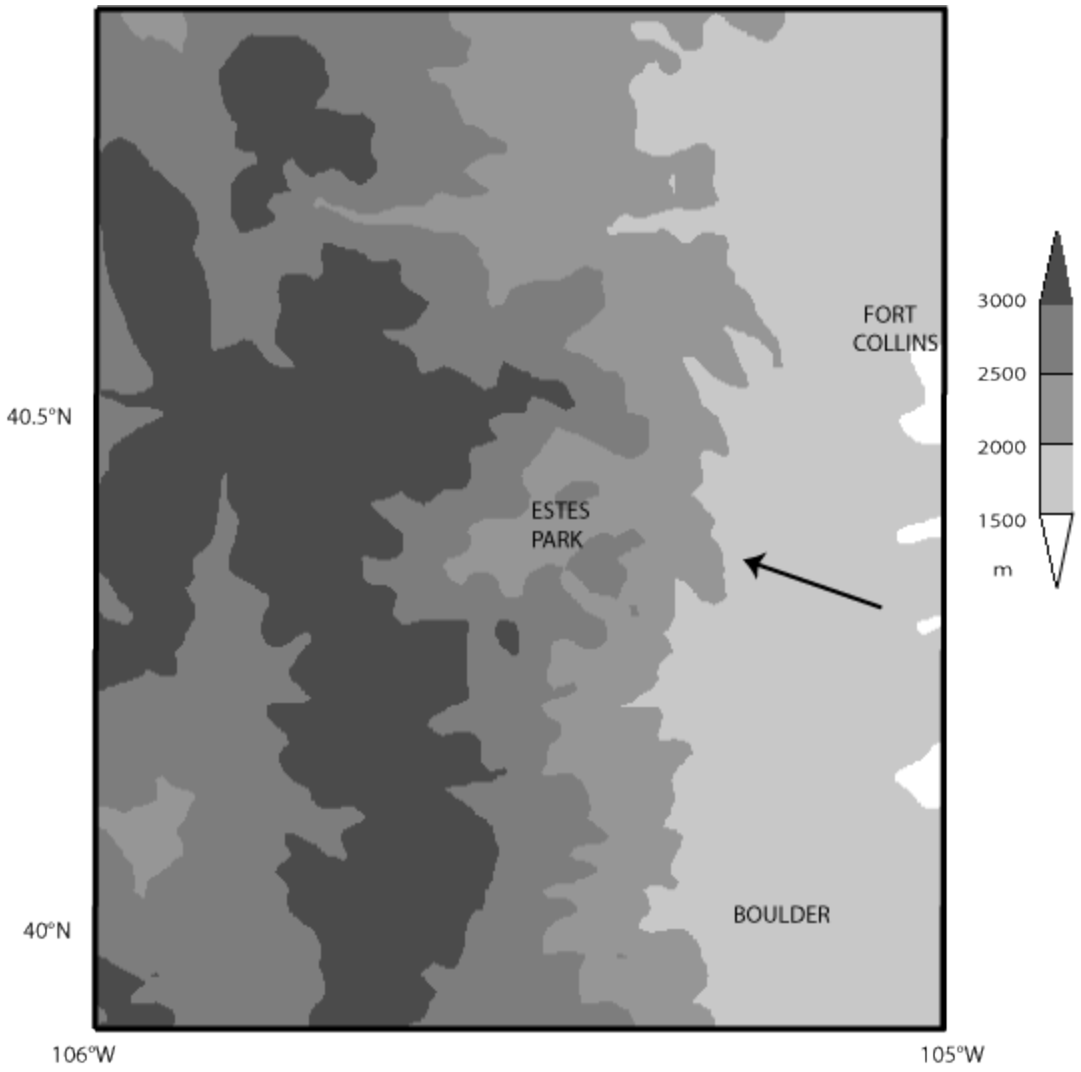

FIG. 1. Topography of the region affected by the Big Thompson flash flood. Terrain contours (m ASL) are shaded. The arrow represents the low-level flow direction.

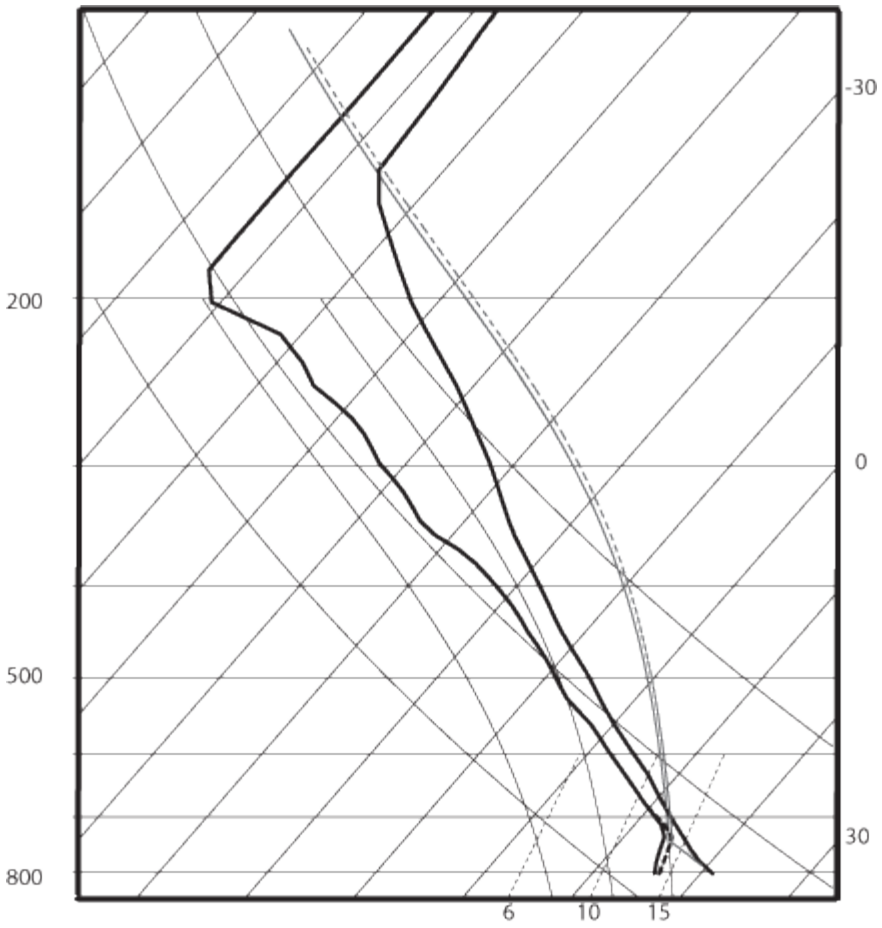

FIG. 2. The idealized profiles of temperature and dew point used in our experiments BIGT3 and BIGT5-7 (solid, thick black lines), BIGT4 and BIGT8-12 (dashed, thick black lines). The bold (respectively, solid and dashed) grey lines represent the pseudo-adiabatic curves of a parcel lifted from the surface.

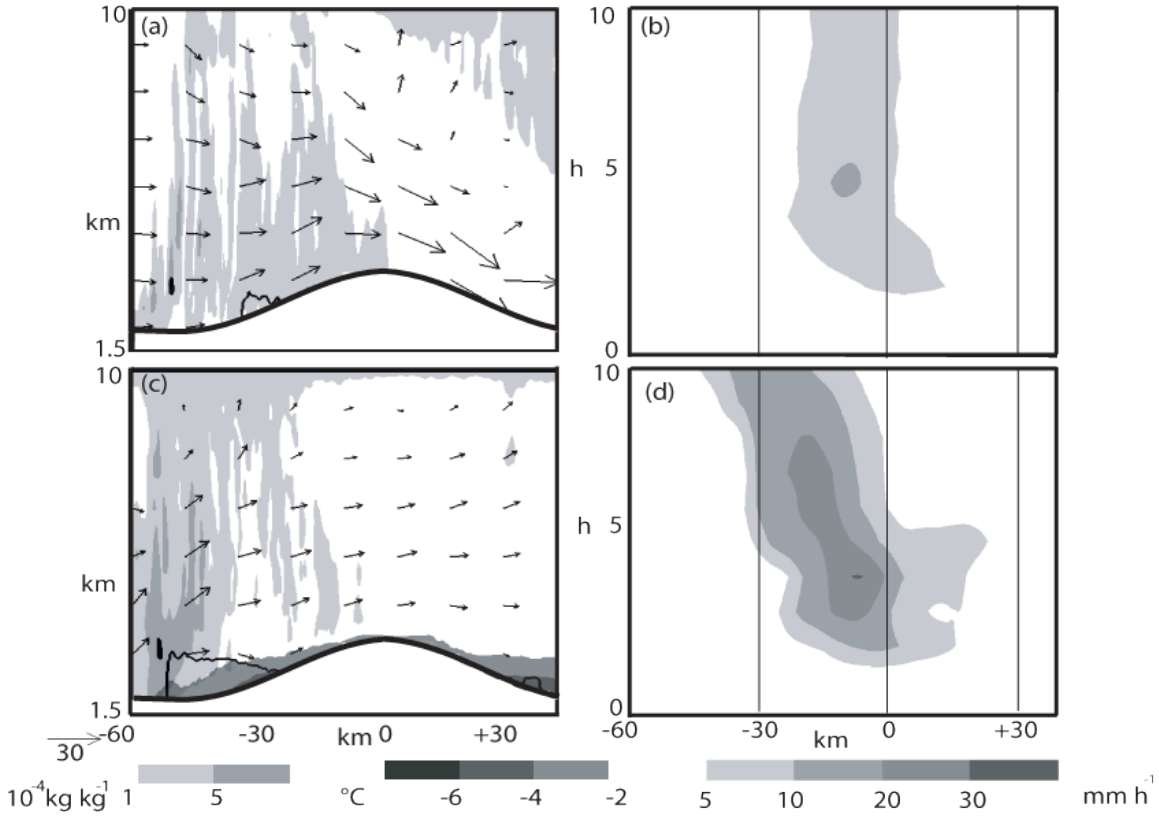

FIG. 3. Left: vertical cross sections of the *y*-average of potential temperature perturbation (dark shaded areas), cloud water plus ice content (light shaded areas), rainwater content (contour line for 0.2×10^{-3} kg kg^{-1}), wind vectors (arrows) for experiments BIGT10 (a, top) and BIGT8 (c, bottom). The results are shown at the final integration time t = 10 h. Right: Hovmöller diagram of the *y*-average of rainrate for experiments BIGT10 (b, top) and BIGT8 (d, bottom). The rainrate is calculated every 1 hour from t = 0 h to t = 10 h. The vertical lines represent the location of the ridge top and half-width.

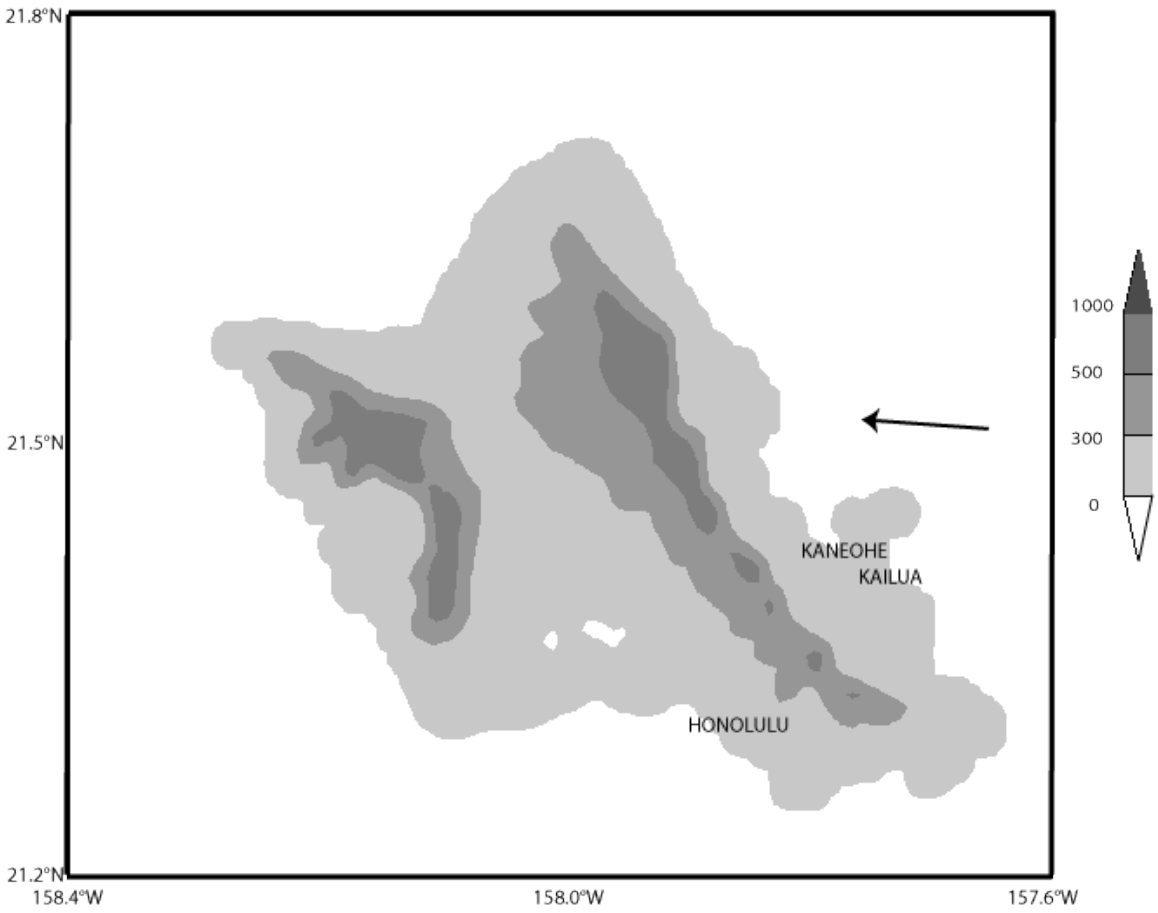

FIG. 4. As Fig. 1, but for the Oahu Flood.

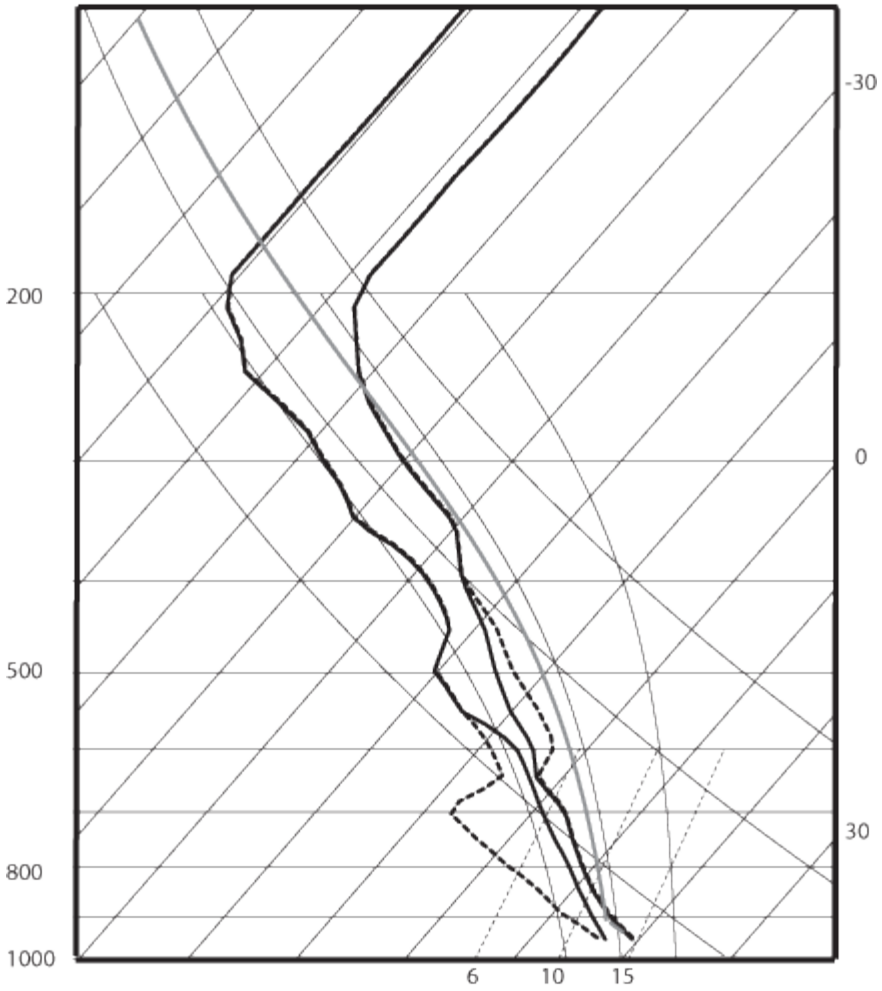

FIG. 5. The idealized profiles of temperature and dew point used in our experiments OAHU4, OAHU5 (solid, thick black lines), and OAHU1 (dashed, thick black lines) (The profiles for Exp. OAHU2 and OAHU3 are a mixture of the two soundings, see text). The bolded grey line represents the pseudo-adiabatic curve of a parcel lifted from the surface in all experiments.

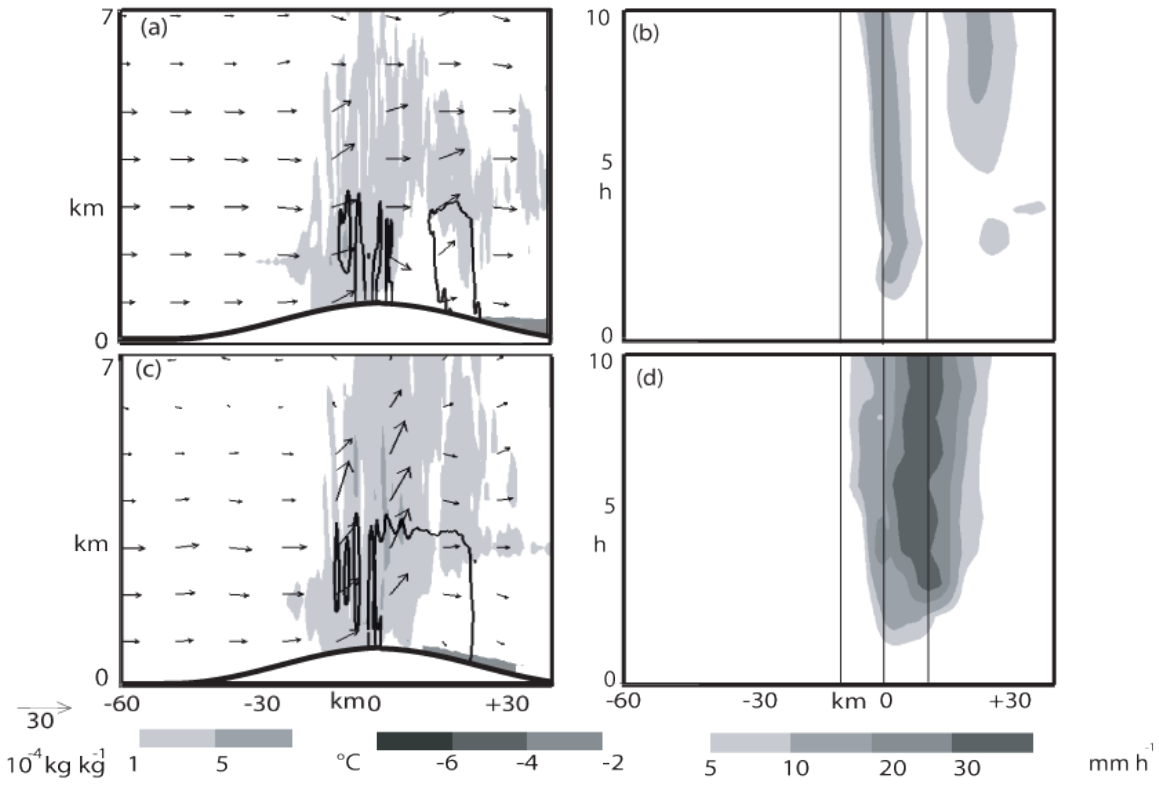

FIG. 6. As Fig. 3, but for experiments OAHU4 (top) and OAHU5 (bottom). Rainwater content contour line is for 0.5×10^{-3} kg kg^{-1}.

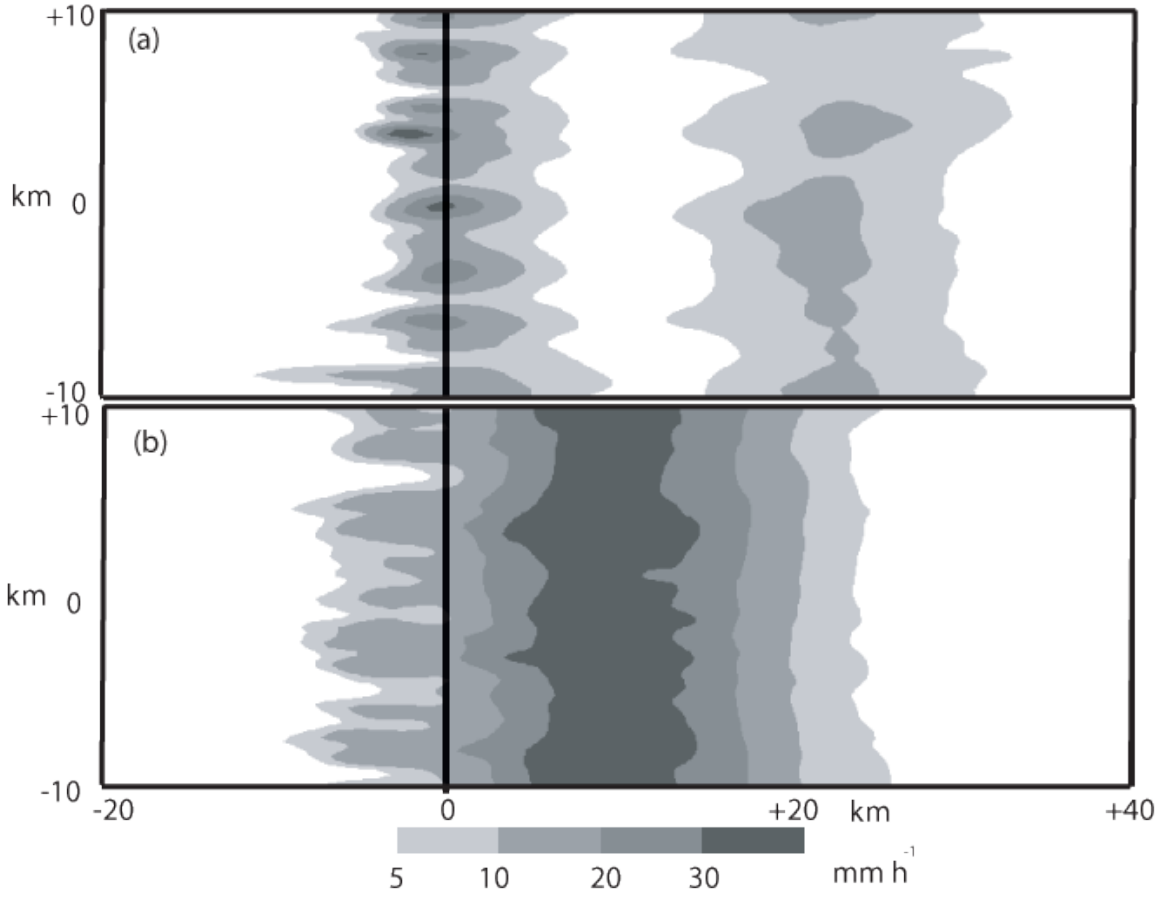

FIG. 7. Rainfall rates simulated near the mountain in experiments OAHU4 (a, top) and OAHU5 (b, bottom). The rainfall is calculated as the hourly average from t = 5 to t = 10 h. The vertical line represents the location of the ridge top.

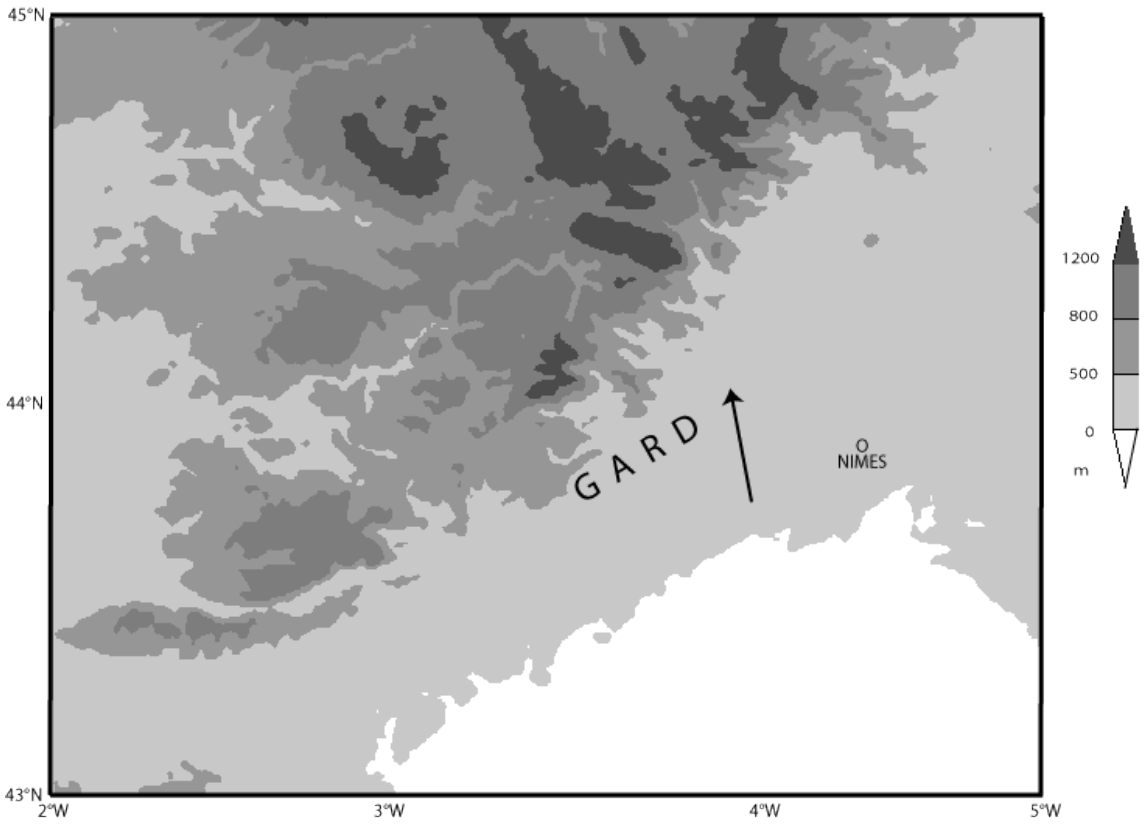

FIG. 8. As Fig. 1, but for the Gard flash-flood.

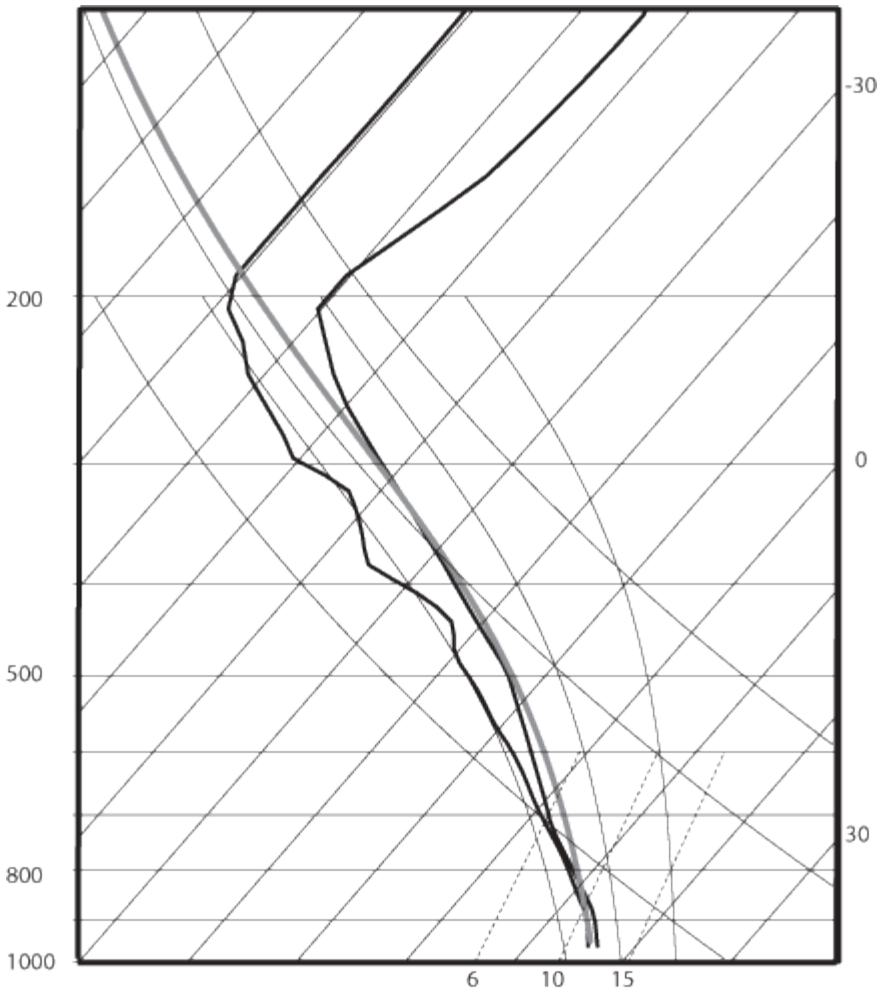

FIG. 9. The idealized profiles of temperature and dew point used in our experiments GARD1-5 (solid, thick black lines). The bolded grey line represents the pseudo-adiabatic curve of a parcel lifted from the surface.

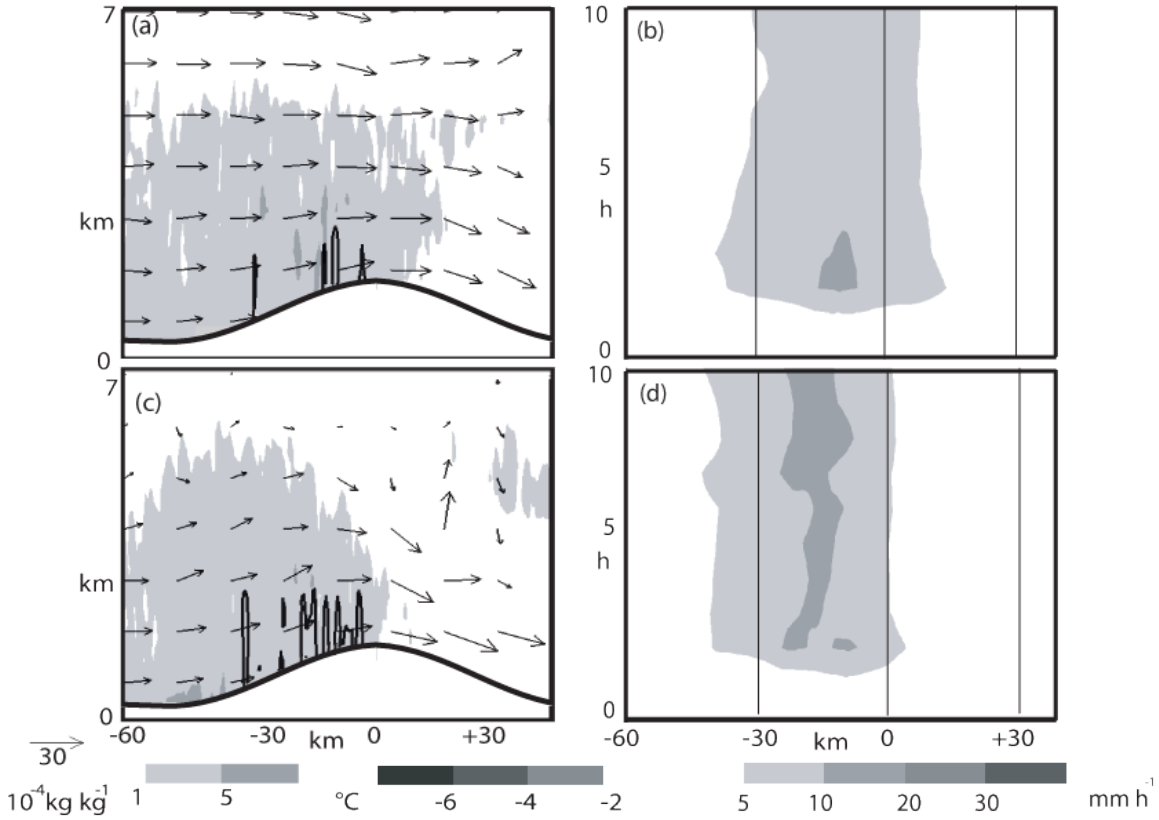

FIG. 10. As Fig. 6, but for experiments GARD2 (top) and GARD3 (bottom)..